ELECTRIC CURRENT PERTURBATION CALCULATIONS FOR HALF-PENNY CRACKS

R. E. Beissner, M. J. Sablik and C. M. Teller

Southwest Research Institute

San Antonio, Texas

INTRODUCTION

The electric current perturbation (ECP) method[1-4] consists of inducing or injecting an electric current flow in the material to be examined and then detecting localized perturbations of the magnetic flux associated with current flow around material defects such as cracks or inclusions. Empirically, ECP data has shown strong correlations among certain signal features and crack size characteristics, and thus promises to be a useful method for quantitative NDE. To aid in the further development of the method, the objectives of the work reported in this paper are (1) to develop a mathematical model of the ECP flux distribution for a half-penny crack, (2) to determine the degree of validity of the model through comparisons with experimental data, and (3) to develop a detailed theory of sizing relationships for half-penny cracks.

SUMMARY OF EXPERIMENTS

Figure 1 shows the basic experimental configuration. The crack length is in the y-direction and the unperturbed current flows in the z-direction perpendicular to the crack face. A differential sensor, consisting of two coils wound on a ferrite rod, is oriented so as to detect magnetic flux density component B_z.

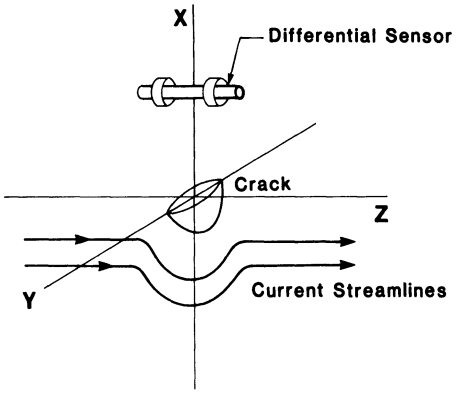

Figure 1. Schematic illustration of the electric current perturbation method

Two types of scans are employed. In one case, the sensor is moved along a track parallel to the z-direction, perpendicular to the crack face. Figure 2a shows typical ECP data for such z-scans at various y-distances from the crack center. In the other type of scan, the sensor, oriented again so as to detect B_z, is moved in the y-direction, parallel to the length of the crack. In this case, data such as those shown in Figure 2b are obtained at various z-distances from the crack.

One notes from Figure 2a that the z-scans are characterized by a large central peak with two smaller, symmetrically placed peaks of opposite sign on either side of the central peak. The central peak is positive for a z-scan on one side of crack center and negative on the other side. For cracks that enter normal to the surface, a z-scan through the center of the crack produces a null signal for all z, as shown here.

From Figure 2b we see that y-scans are characterized by double peaks of opposite sign with a zero at y=0. The double peaks exhibit maximum amplitude for a y-scan which is directly over the crack itself.

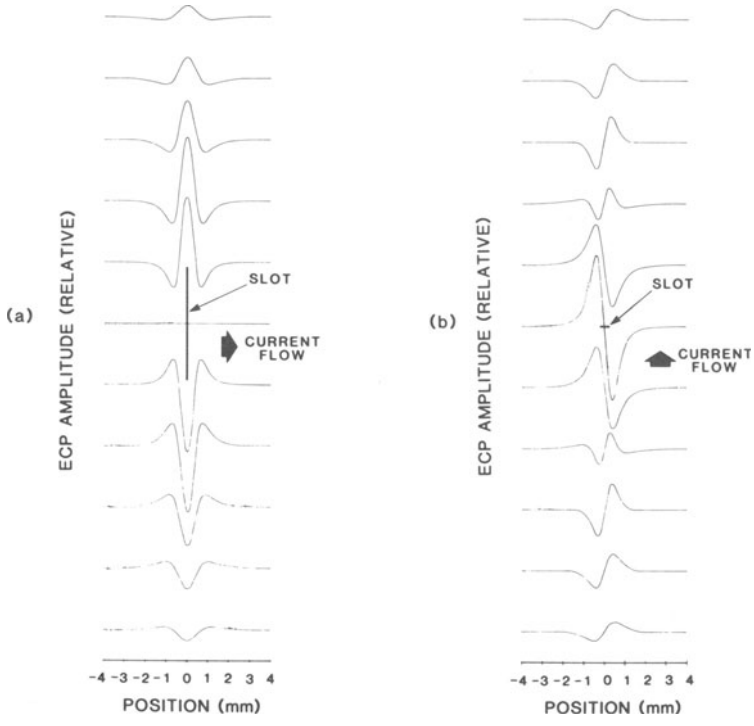

Figure 2. Typical electric current perturbation data for a slot entering normal to the surface. Data in (a) are obtained from scans in the z-direction of Fig. 1, while (b) is obtained from scans in the y-direction

It is the y-scan data that are used for crack characterization. Empirically it is found that the peak-to-peak distance is linearly related to crack length while the peak-to-peak amplitude is very nearly proportional to crack area.[5] One of the aims of the modeling effort described below is to investigate these crack characterization relationships in more detail.

THE BASIC MODEL

Figure 3 shows the geometrical model used for the half-penny crack. The crack is modeled as an elliptical opening of minor radius a and major radius b with eccentricity $e = \sqrt{1-(a/b)^2} \approx 1$. Since the crack face is a half-circle, the crack is seen to be half of an extremely oblate spheroid.

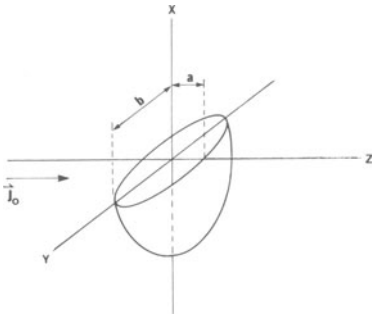

Figure 3. Geometrical model of a half-penny crack

In most experimental situations of interest, we are working with low conductivity materials at low frequencies and are interested in detecting small cracks. Thus, we assume at the outset that skin depth >> crack depth, so that we can take the unperturbed current density to be uniform.

Under these conditions, the calculation of current flow around the crack is exactly the same as the calculation of fluid flow around an obstacle of the same shape. The hydrodynamic problem, namely that of flow around an oblate spheroidal obstacle, has already been solved.[6] We thus use that solution to write expressions for the perturbed current.

Using oblate spheroidal coordinates, as given by[7]

$$x = \rho\cos\phi = be(1+\sigma^2)^{1/2}\,(1-\tau^2)^{1/2}\,\cos\phi \quad , \tag{1a}$$

$$y = \rho\cos\phi = be(1+\sigma^2)^{1/2}\,(1-\tau^2)^{1/2}\,\sin\phi \quad , \tag{1b}$$

$$z = be\sigma\tau, \tag{1c}$$

we rewrite Kennard's expressions[6] for j_σ, j_τ, j_ϕ using transformation formulae from Korn and Korn[7] and obtain for the components of the change in current density caused by the crack:

$$\Delta j_x = j_x = -g_2 j_o \sqrt{\frac{1-\tau^2}{1+\sigma^2}}\,\frac{\tau}{\sigma^2+\tau^2}\cos\phi \quad , \tag{2a}$$

$$\Delta j_y = j_y = -g_2 j_o \sqrt{\frac{1-\tau^2}{1+\sigma^2}} \frac{\tau}{\sigma^2+\tau^2} \sin\phi \quad , \tag{2b}$$

$$\Delta j_z = j_z - j_o = g_2 j_o \left\{ \frac{\sigma}{\sigma^2+\tau^2} - \tan^{-1}\frac{1}{\sigma} \right\} \quad . \tag{2c}$$

Here, j_o is the unperturbed current density and

$$g_2 = \frac{1}{\tan^{-1}\frac{1}{\sigma_o} - \frac{\sigma_o}{1+\sigma_o^2}} \quad , \tag{3}$$

where $\sigma_o e = \sqrt{1-e^2}$, and where $\sigma=\sigma_o$ is the equation for the crack surface.

The next step is to calculate the perturbation in the vector potential from these current perturbations and then take the curl to find the flux density.

Because we are interested mostly in small cracks, we expect that the current density change produced by a crack will be significant only at a small distance r' from the center of the crack. This suggests that a multipole or spherical harmonics expansion of the vector potential might be useful. In particular, the vector potential is expressed as

$$A_i = \mu_o \sum_{\ell,m} \frac{1}{2\ell+1} f^i_{\ell m}(r) Y_{\ell m}(\theta,\phi) \quad , \tag{4}$$

where i = x,y, or z, μ_o is the permeability of free space, and the coefficients are

$$f^i_{\ell m}(r) = \frac{1}{r^{\ell+1}} \int_o^r \int_{-1}^1 \int_o^{2\pi} r'^{\ell+2} j_i(r',\theta',\phi') Y^*_{\ell m}(\theta',\phi') d\phi' d\mu' dr'$$

$$+ r^{\ell} \int_r^{\infty} \int_{-1}^1 \int_o^{2\pi} \frac{1}{r'^{\ell-1}} j_i(r',\theta',\phi') Y^*_{\ell m}(\theta',\phi') d\phi' d\mu' dr' . \tag{5}$$

We relate r and θ to the oblate spheroidal coordinates as follows:

$$r = \sqrt{\rho^2+z^2} = be\sqrt{1+\sigma^2-\tau^2} \quad , \tag{6a}$$

$$\cos\theta = \mu = z/r = \sigma\tau/\sqrt{1+\sigma^2-\tau^2} \quad , \tag{6b}$$

$$\sin\theta = \left[(1+\sigma^2)(1-\tau^2)/(1+\sigma^2-\tau^2)\right]^{1/2} \quad . \tag{6c}$$

From this point on, we have completed the calculation in two different ways involving different approximations in the multipole expansion.

THE LARGE r/b APPROXIMATION

In our first calculation, we assume that r, the distance from the crack to the sensor, is large compared to b, the crack radius, and use this approximation to simplify the volume integrals in equation (5). In particular, we assume that r is large enough that we may approximate the spherical surface r=constant by an ellipsoidal surface σ=constant. Because τ varies from -1 to +1, we see from equation (6a) that on the ellipsoidal surface the minimum r is beσ whereas the maximum r is be$\sqrt{1+\sigma^2}$. Thus, the approximation amounts to the assertion that

$$\frac{r_{min}}{r_{max}} = \frac{\sigma}{\sqrt{1+\sigma^2}} \simeq 1.$$

Even with σ as small as 2, the ratio $r_{min}/r_{max} \simeq 0.89$. Thus, for large r/b, the spherical surface r=constant may be replaced by the spheroidal surface $\sigma \simeq r/be$ = constant.

The integrals in equation (5) are then written in terms of spheroidal coordinates as follows:

$$f^i_{\ell m}(\xi) = \frac{(be)^2}{\xi}\Big\{\frac{1}{\xi^\ell}\int_0^\xi d\sigma\int_1^1 d\tau\int_{\pi/2}^{3\pi/2} d\phi\,(1+\sigma^2-\tau^2)^{\ell/2}(\sigma^2+\tau^2)$$

$$\times\, j_i(\sigma,\tau,\phi)Y^*_{\ell m}(\theta,\phi)$$

$$+\ \xi^{\ell+1}\int_\xi^\infty d\sigma\int_{-1}^1 d\tau\int_{\pi/2}^{3\pi/2} d\phi\ (\sigma^2+\tau^2)/(1+\sigma^2-\tau^2)^{(\ell+1)/2}$$

$$\times\, j_i(\sigma,\tau,\phi)Y^*_{\ell m}(\theta,\phi)\ \Big\}, \tag{7}$$

where $\xi = r/be$.

We here restrict ourselves to the dipole approximation, which means that the expansion in equation (4) is restricted to $\ell \leq 1$. We find that the only nonvanishing coefficients in the remaining terms are f^z_{00}, f^x_{10}, and $f^z_{11} = -f^z_{1-1}$. Analytical expressions can be

obtained for f^z_{00} and f^x_{10}, but f^z_{11} can at best be reduced to a single integral which must then be evaluated numerically. As it turns out,

$$B_z = \frac{\partial A_y}{\partial x} - \frac{\partial A_x}{\partial y} = \frac{\mu_o}{3}\sqrt{\frac{3}{4\pi}}\left(\frac{yz}{r^2}\right)\frac{1}{be}\left[\frac{\partial f^x_{10}}{\partial \xi} - \frac{1}{\xi} f^x_{10}\right] , \qquad (8)$$

where

$$f^x_{10} = \sqrt{\frac{3}{\pi}}\, j_o g_2 \frac{(be)^2}{\xi}\left\{\frac{\pi}{8\xi}\left[\sqrt{1+\xi^2} - \sqrt{1+\sigma_o^2}\right]\right.$$

$$\left. + 2\xi^2\left[(1+\xi^2)\left(E(k)-K(k)\right)+K(k)-\frac{\pi}{4}\right]\right\}, \qquad (9)$$

with $K(k)$ and $E(k)$ being complete elliptic integrals of the first and second kind, respectively, and where $k=1/\sqrt{1+\xi^2}$. Thus, the $\vec{B}$-component of interest can be expressed completely analytically.

INCLUSION OF HIGHER MULTIPOLES

The second way we have done the calculation is to evaluate the volume integrals in equation (5) numerically. This is not as difficult as it might seem because the ϕ-variable integrates analytically so that all that is left is a double integral. Further, since we are interested in B_z, we need only evaluate $f^x_{\ell m}$ and $f^y_{\ell m}$, which differ by a constant factor and are functions only of the dimensionless variable ξ. Thus, we need to evaluate one of the functions $f^x_{\ell m}$ or $f^y_{\ell m}$ only once to provide the data needed for all crack sizes.

In particular, expressing the spherical harmonics in terms of associated Legendre polynomials $P_\ell^m(\mu)$ as $Y_{\ell m}(\mu,\phi)=N_{\ell m}P_\ell^m(\mu)e^{im\phi}$, we find that

$$f^{x,y}_{\ell m} = \alpha^{x,y}_{\ell m}\left\{\frac{1}{\xi^{\ell+1}}\int_0^\xi d\xi' \int_{-1}^1 d\mu\, \xi'^{\ell+2}\sqrt{\frac{1-\tau^2}{1+\sigma^2}}\frac{\tau}{\sigma^2+\tau^2}P_\ell^m(\mu)\right.$$

$$\left. + \xi^\ell \int_\xi^\infty d\xi' \int_{-1}^1 d\mu \sqrt{\frac{1-\tau^2}{1+\sigma^2}}\frac{\tau}{\sigma^2+\tau^2}\frac{P_\ell^m(\mu)}{\xi'^{\ell-1}}\right\} , \qquad (10)$$

where

$$\sigma^2 = \frac{1}{2}\left\{\xi'^2-1 + \left[(\xi'^2-1)^2+4\xi'^2\mu^2\right]^{1/2}\right\} , \qquad (11a)$$

$$\tau = \xi'\mu/\sigma \quad . \tag{11b}$$

For m = 1 we find

$$\alpha^x_{\ell 1} = \frac{\pi}{2} N_{\ell 1} = i\alpha^y_{\ell 1} \tag{12a}$$

while for even m ≠ 1,

$$\alpha^x_{\ell m} = (-1)^{m/2} \frac{2}{m^2-1} N_{\ell m} = i\alpha^y_{\ell m} \quad , \tag{12b}$$

and for odd m, $\alpha^x_{\ell m} = \alpha^y_{\ell m} = 0$. We also have that

$$N_{\ell m} = (-)^m \sqrt{\frac{(2\ell+1)}{4\pi} \frac{(\ell-m)!}{(\ell+m)!}} \quad . \tag{13}$$

The integrals in eq. (10) have been evaluated numerically for all non-vanishing coefficients through ℓ=7.

COMPARISON WITH EXPERIMENT

To compare with experiment, where a differential sensor is used, we evaluate

$$\Delta B_z = B_z(x,y,z_o + \frac{1}{2}z) - B_z(x,y,z_o - \frac{1}{2}z) \quad . \tag{14}$$

Further, this result is integrated across the cross sections and lengths of the probe coils to obtain an averaged result $\Delta B_z(z_o)$. In our calculation, we assumed that the crack had an eccentricity of 0.999.

Figure 4 shows comparison of the large r/b approximation with experimental z-scans at various distances from the center of the crack for a crack of 0.76 mm length. Because we do not have absolute measurements of flux density, we have normalized theoretical and experimental amplitudes for the scan in the center of the figure and have used this same normalization factor to compute signal traces at the other y-distances from crack center and for other crack lengths from 0.25 to 1.30 mm.

Figure 5 shows results for the 0.25 mm crack. We expect to get good agreement like this for small cracks because b is small and the sensor is at positions of large r/b, as assumed. At the other extreme, for a 1.02 mm crack, the theory is not expected to do as well, as seen in Figure 6. Overall, however, agreement with experiment is

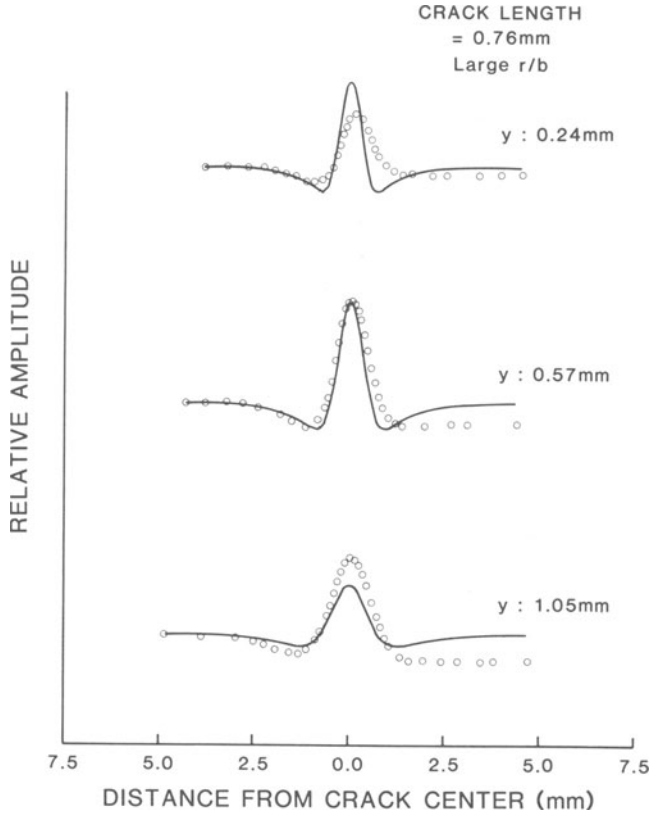

Figure 4. Comparison of measured flux densities with calculations based on the large r/b approximation for a crack 0.76 mm in length. The solid curve is calculated and the points are experimental data.

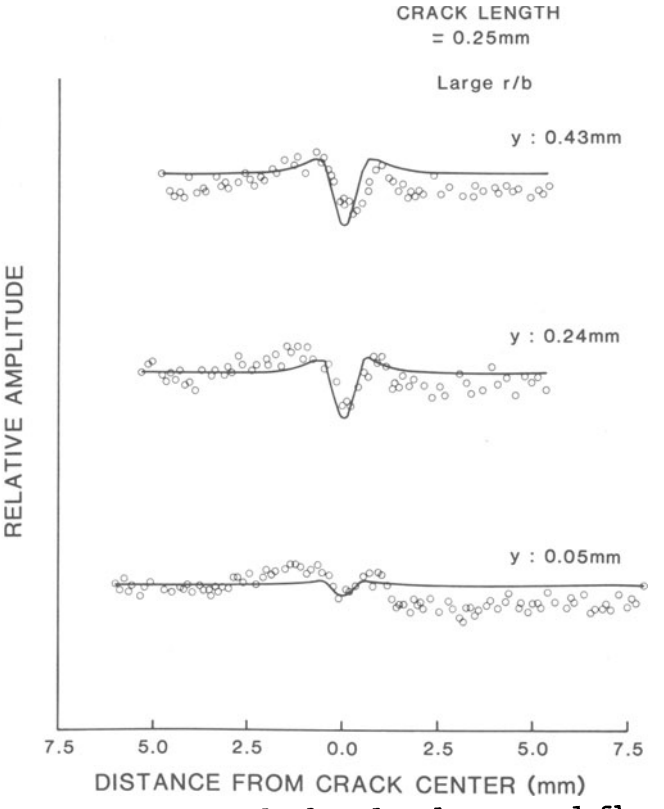

Figure 5. Calculated and measured flux densities for a 0.25 mm crack

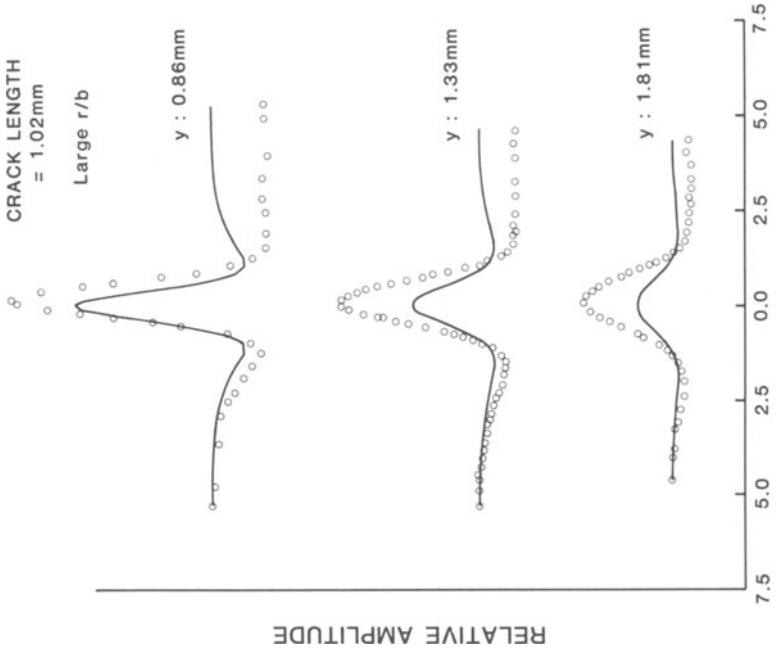

Figure 6. Calculated and measured flux densities for a 1.02 mm crack

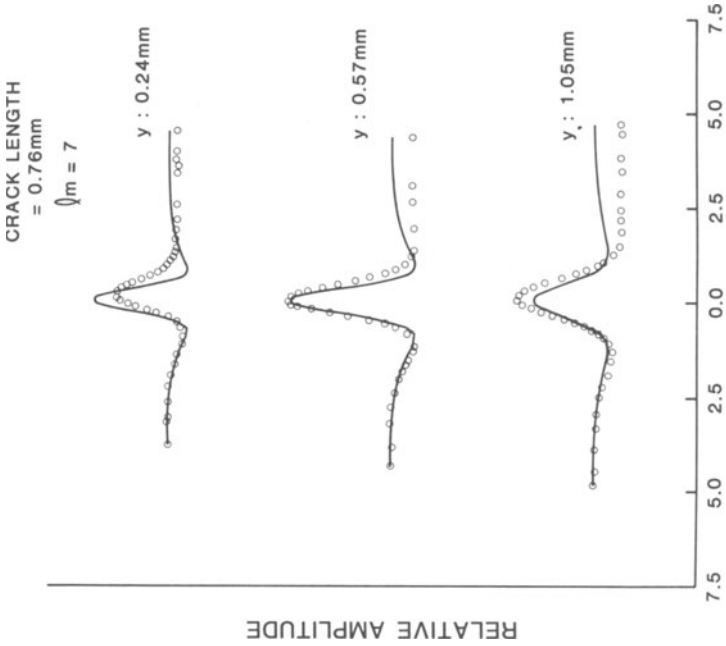

Figure 7. Comparison of measured flux densities with higher order calculations

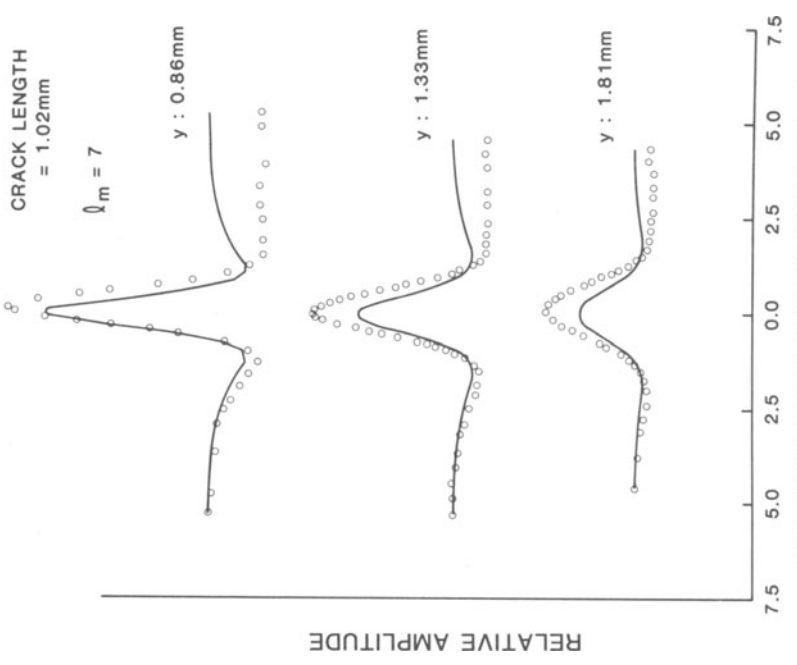

Figure 9. Calculated and measured data for a 1.02 mm crack

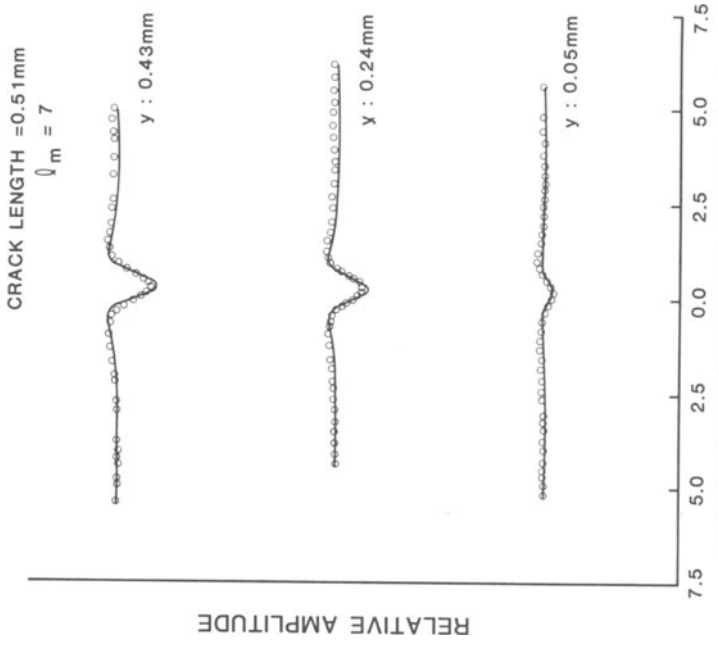

Figure 8. Calculated and measured data for a 0.51 mm crack

actually better than expected, considering the nature of the large r/b approximation. We therefore expect this simple analytic solution to prove useful in future studies of ECP probe optimization.

Comparisons between experimental z-scans and the higher order multipole calculations through $\ell = 7$ have also been obtained. Figure 7 displays the results for a 0.76 mm crack. For these calculations we determined a new normalization factor, again from the trace in the center of the figure. This new normalization was used for calculations at 0.51 mm, which are shown in Figure 8, and for 1.02 mm, which are shown in Figure 9. The higher order numerical treatment gives better agreement, particularly at the larger crack length of 1.02 mm, as it should. The results, however, still show a slight departure from experiment for the larger crack lengths.

As we mentioned earlier, we are interested in crack sizing relationships. Experiment exhibits an approximately linear relationship between crack length and peak-to-peak separation in the y-scan at z = 0 (i.e. along the length of the crack and directly over the crack). We see this in Figure 10, where the experimental points are designated by crosses. Also displayed are the large r/b approximation and the higher order multipole calculations through $\ell = 1$ and $\ell = 7$. There is no normalization involved here; the calculated and experimental peak-to-peak separations agree at the smallest crack length in all cases.

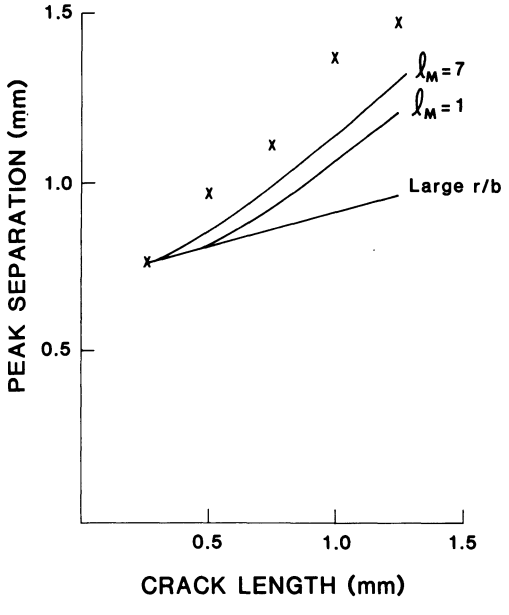

Figure 10. Peak-to-peak separation distance obtained from y-direction scans as a function of crack length. The solid curves are calculated and the points are experimental.

In looking at the results for $\ell = 1$ and $\ell = 7$, it would appear that all we have to do is add more terms to obtain agreement with experiment because the trend in going from $\ell = 1$ to $\ell = 7$ is toward better agreement. Actually, we do need to carry more terms because we have looked at the convergence of the sum for a 1.30 mm crack and have determined that peak separation is still changing appreciably when we add the $\ell = 7$ term.

There are, however, other possible reasons for the difference between theory and experiment. For example, one point of concern was that the coils were wound on a ferrite core for the experimental measurements while the calculations did not account for the presence of permeable material in the sensor. However, recent experimental data shown in Figure 11 indicate that the principal effect of the ferrite core is to increase the amplitude of the signal with no significant change in peak position. It is therefore unlikely that the omission of a permeable core in the analytical model is responsible for the differences in peak-to-peak distance shown in Figure 10.

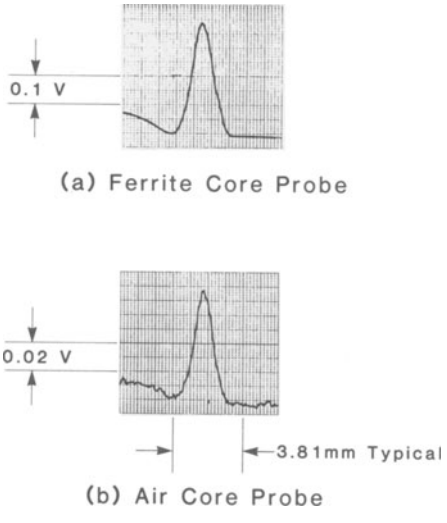

Figure 11. Experimental data obtained with sensors with and without a ferrite core

Another possibility is related to the experimental geometry in which the specimen was cylindrical and the crack was circumferential. Thus, in the actual experiment the surface in the y-direction along

the crack length was curved. We expect the effect of curvature to be more important for the larger length cracks, and, as we observe, the discrepancy between theory and experiment is indeed greater for the larger length cracks.

Figure 12 focuses on the other sizing relationship - namely that between signal amplitude and crack area. In this figure the three theoretical predictions were plotted first. Then the experimental data were normalized to coincide with the theoretical predictions of $\ell = 1$ and $\ell = 7$ for the 0.51 mm crack. Again, we see some disagreement for the longer length cracks, which is probably associated with the same uncertainties as in the peak separation-crack length comparison.

Thus, we conclude that for small, half-penny cracks, the analytical model presented here provides a good account of both the detailed behavior of ECP signals and empirically determined sizing relationships. This being the case, we now have a sound basis for proceeding with applications to probe optimization and for extensions of the theory to other flaw geometries.

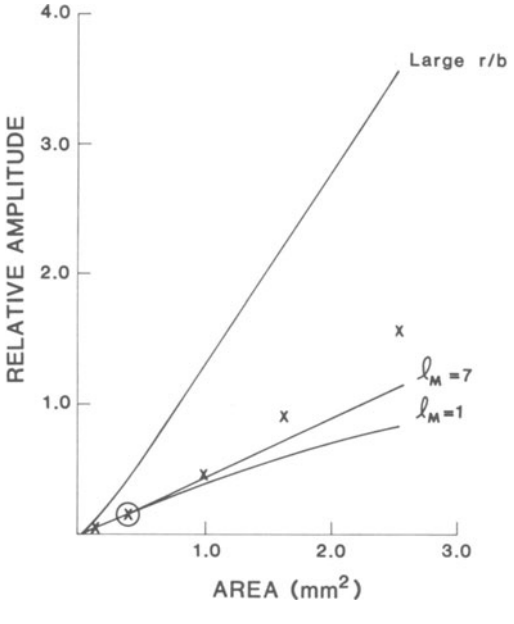

Figure 12. Peak amplitude vs. crack area as obtained from y-direction scans. The experimental data are normalized at the circled point.

SUMMARY

We have used a solution from hydrodynamics to calculate the current flow around a half-penny crack, and then a multipole expansion of the vector potential to calculate the corresponding change in flux density. We are quite pleased with the overall agreement between theory and experiment, particularly for smaller crack sizes, which are our principal concern. As higher and higher order multipole terms are used for the vector potential, the trend appears to confirm the sizing relationships that have been established experimentally - namely that for scans along the length of the crack, peak-to-peak separation vs. crack length is a linear relationship and signal amplitude vs. crack area is also roughly linear.

ACKNOWLEDGEMENTS

The authors are indebted to G.L. Burkhardt for many invaluable discussions and for experimental support. We also extend our thanks to M. Kilman for his able assistance in running some of the computer plots and to J. Blanton for digitizing the experimental data. This work was sponsored by the Center for Advanced Nondestructive Evaluation, operated the the Ames Laboratory, USDOE, for the Air Force Wright Aeronautical Laboratories/Materials Laboratory and the Defense Advanced Research Projects Agency under Contract No. W-7405-ENG-82 with Iowa State University.

REFERENCES

1. R. E. Beissner, C. M. Teller, G. L. Burkhardt, R. T. Smith and J. R. Barton, "Detection and Analysis of Electric Current Perturbation Caused by Defects," Proc. Symposium on Eddy Current Characterization of Materials and Structures, Gaithersburg, MD, ed by G. Birnbaum and G. Free, ASTM STP 722 (1981), pp. 428-446.
2. C. M. Teller and G. L. Burkhardt, "Small Defect Characterization by the Electric Current Perturbation Method," Proc. 13th Symposium on NDE, San Antonio, TX, ed by B. E. Leonard (NTIAC, San Antonio, TX, 1981), pp. 443-453.
3. C. M. Teller and G. L. Burkhardt, "Detection and Characterization of Defects by the Electric Current Perturbation Method," Proc. DARPA/AFML Review of Progress in Quantitative NDE (LaJolla, CA, 1981).
4. C. M. Teller and G. L. Burkhardt, "NDE of Fastener Hole Cracks by the Electric Current Perturbation Method," Proc. DARPA/AFML Review of Progress in Quantitative NDE (LaJolla, CA, 1981).
5. F. N. Kusenberger, P. H. Francis, B. E. Leonard and J. R. Barton, "Nondestructive Examination of Metal Fatigue," AFOSR 69-1429TR (1969), AD688892.

6. E. H. Kennard, "Irrotational Flow of Frictionless Fluids, Mostly of Invariable Density," David Taylor Model Basin, USN Report 2299, NTIS AD 652463, pp. 346-369.
7. G. A. Korn and T. M. Korn, Mathematical Handbook for Scientists and Engineers, (McGraw-Hill, NY, 1961), Chapter 6.

DISCUSSION

D.H. Michael (University College London): I was curious to know why, when you start with the exact solution to the problem, you are using approximations. Couldn't you complete the whole thing in the terms of exact solutions?

R.E. Beissner (Southwest Research Institute): The exact solution is just for the change in current density. What I need to know is the magnetic field strength. But that's where things get difficult because the integral is quite complicated. So we used approximations to do the integrations required to get the vector potential and then from that, the flux density. If all I wanted to know was the current density, there would be no approximation, but that's not what we measured. We measured the flux density.

D.H. Michael: What's the real difficulty, then? Working out the integral?

R.E. Beissner: Right.

D.H. Michael: So you have to go to an approximation?

R.E. Beissner: That's it, essentially.

J.A. Baines (AMF Tuboscope): I noticed that in your paper your experimental data were consistently asymmetric as you went across the crack, whereas your calculated data were not. Can you speak to this? Is that because the data were not take quasistatically? Or is that some effect that's not taken into account in the theory?

R.E. Beissner: The theory, of course, assumed a perfectly symmetric crack, and that's why everything was symmetric. From previous experiments when we see this kind of asymmetry in the signal, it is a sign that the crack is not entering normally or has something in its geometry that isn't perfectly symmetric. Almost all cracks have something like that. That's rather typical of a crack.

J.A. Bains: These were natural flaws, then?

R.E. Beissner: yes, that's right. These were fatigue cracks grown in titanium.

J.A. Bains: All right. You did verify that and it doesn't depend on scan direction? It is not a time factor, it's actually a distance factor?

R.E. Beissner: You mean going this way or back that way? No, we get the same thing. It is true asymmetry.

C.M. Teller (Southwest Research Institute): I might say a word about that, since we were the ones who generated the experimental data. There are some dynamics of probe motion involved in the asymmetry, and those dynamics have not been truly well quantified. The data that you saw there were data digitized from strip chart recordings, and there is also some error involved in that process. I don't believe that's the cause of the asymmetry, but that showed some of the scatter that wasn't apparent from the analog traces. The distortion in the experimental data can be due to experimental procedure, and that is one thing that has to be carefully guarded against.

A.J. Bahr (SRI International): I noticed that in the data that you showed to compare with theory there was no noise, but on the bolt hole there is a background as you rotate around it. Is that background essentially a lift-off effect?

C.M. Teller: In the work that we did on the smooth bar fatigue specimen, the variation in the background is not due to lift-off. We control lift-off very carefully in those experiments and, in fact, the background is very reproducible. I presented some work here two years ago on the work that we did on the bolt hole with the electric current probe. If you recall from those data, the background signals repeated, I would say, almost exactly. That's a material contribution to the signal. The electronic noise, lift-off, all of those parameters, in fact, have been very carefully controlled. With regard to the titanium results that I showed, there are some contributions to the background, the random contributions to the background that possibly are there due to lift-off, but they are very minor in comparison to the background from the material.

A.J. Bahr: Would you say that qualitative lift-off sensitivity is not a problem then?

C.M. Teller: It hasn't been a problem with the approach that we've taken using the tangential component of the flux leakage and differentially detecting that component. With other approaches, I believe it could be a problem. Those are some of the things that we need to continue to investigate.

D.H. Michael: I wonder whether you have the same difficulty as UCL had in sampling the crowns of threads when you are dealing with threads, because I think one of the sources of scatter in the data that we have here is caused by the fact that probes at the thread tops do want to wobble off either one way or the other. That is part, I think, of the scatter that we find in the experimental data.

C.M. Teller: In any real system, I believe that could be a problem that would have to be addressed, and it would involve some degree of precision in respect to the pitch of the probe scan with relation to the threads and, of course, taking into account the tolerance on those threads. These happen to be very high precision threads as is the case, I'm sure, on the space shuttle bolts. But those effects are the things that engineering or application engineering will need to address in really bringing these methodologies to fruition in terms of production or field use. I know we are all thinking in terms of applications these days, but we need to have some very good fundamental tools to work with to apply to these problems, and we need to look at those aspects in this program.